XXV CONGRESO DE ECUACIONES DIFERENCIALES Y APLICACIONES
XV CONGRESO DE MATEMÁTICA APLICADA
DEL 26 AL 30 DE JUNIO DE 2017
CEDYA+CMA
XXV CONGRESO DE ECUACIONES DIFERENCIALES Y APLICACIONES
XV CONGRESO DE MATEMÁTICA APLICADA
CARTAGENA - 2017

Combined in-silico and on-chip validation of aggressive behaviors developed after vaso occlusions in brain tumors

A. Martínez-González[*], J.M. Ayuso[†], R. Monge[‡], M. Virumbrales-Muñoz[‡], G. A. Llamazares[‡], A. Hernández-Laín[§], P. Sánchez-Gómez[¶], V. M. Pérez-García[*], I. Ochoa[‡] and L. J. Fernández[‡]

Abstract— Glioblastoma (GBM) is the most malignant and most common primary brain tumor. Hypercellular regions surrounding necrotic areas in GBM, named pseudopalisades, are characteristic of these tumors and have been hypothesized to be waves of migrating GBM cells. The universal appearance of these structures in GBM suggests that they may play an instrumental role in their spreading and invasion. A mathematical model was developed incorporating the main mechanisms of pseudopalisade formation. It consists of a set of partial differential equations modeling the interplay of 3 cellular cancer cell phenotypes, the oxygen distribution and necrosis. Experiments were done by embedding different densities of U-251 MG cells within a collagen hydrogel in a custom-designed microfluidic device. By controlling the medium flow through lateral microchannels, we mimicked and controlled blood-vessel obstruction events associated with this disease. Using a combination of computational and experimental techniques, we proved the feasibility of the two hypotheses of pseudopalisade formation: driven by either acute or chronic hypoxia. Additionally, we verified the potential of microfluidic devices as advanced artificial systems capable of experimentally modeling nutrient and oxygen gradients during tumor evolution.

Keywords: brain tumor, mathematical model, microfluidic devices, aggressive behavior.

1 Introduction

Glioblastoma (GBM) is the most common and lethal malignant primary brain tumor. Patients receiving the standard-of-care based on local radiotherapy and concomitant chemotherapy have a median survival of 14 months [1]. GBM tumors are highly infiltrating and fast progressing tumors and are characterized by two main histopathological conditions: necrotic foci typically surrounded by areas of high cellularity known as pseudopalisading regions, and microvascular proliferation. These hypercellular regions surrounding necrotic areas, named pseudopalisades have been hypothesized to be waves of migrating GBM cells [2]. The universal appearance of these structures suggests that they may play an instrumental role in their spreading and invasion. These structures are thought to be induced by oxygen depletion caused by the accumulation of cells far from nutrient supplies (chronic hypoxia) and/or tumor-induced blood vessel occlusion (acute hypoxia) [3]. Both cases are represented in immunohistochemical analysis in Fig. 1.

[*]Laboratorio de Oncología Matemática. Departamento de Matemáticas, Universidad de Castilla-La Mancha, ETSI Industriales, Ciudad Real, 13005 (Spain). Email: alicia.martinez@uclm.es

[†]Morgridge Institute for Research, 330 N Orchard street, Madison, WI, USA. 53715. Wisconsin Institutes for Medical Research, 1111 Highland Ave, Madison, WI 53705.

[‡]Group of Structural Mechanics and Materials Modelling (GEMM). Centro Investigación Biomédica en Red. Bioingeniería, Biomateriales y Nanomedicina (CIBER-BBN), Zaragoza, Spain. Aragón Institute of Engineering Research (I3A), University of Zaragoza, Zaragoza, Spain. Aragon Institute of Biomedical Research, Instituto de Salud Carlos III, Zaragoza, Spain.

[§]Department of Pathology (Neuropathology), Hospital Universitario 12 de Octubre Research Institute, Madrid, Spain

[¶]Neuro-oncology Unit. Health Institute Carlos III-UFIEC, Madrid, Spain.

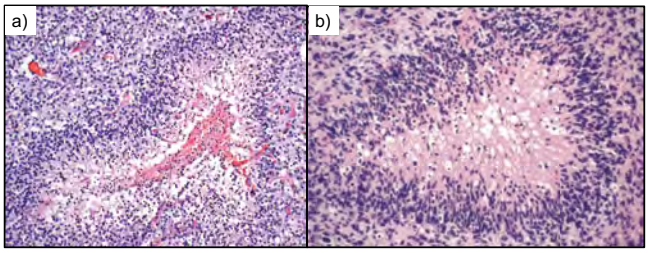

Figure 1: Histopathologic features of pseudopalisades in glioblastoma (GBM). a) tumor cells appear to be migrating away from centrally degenerating vessels and toward alternative vascular supplies. b) Medium-sized pseudopalisades (200-400 μm) are characterized by central necrosis, central vacuolization, and individual dying cells but typically have a peripheral zone of fibrillarity immediately inside the pseudopalisade. Note the absence of central vessels or vascular thrombosis.

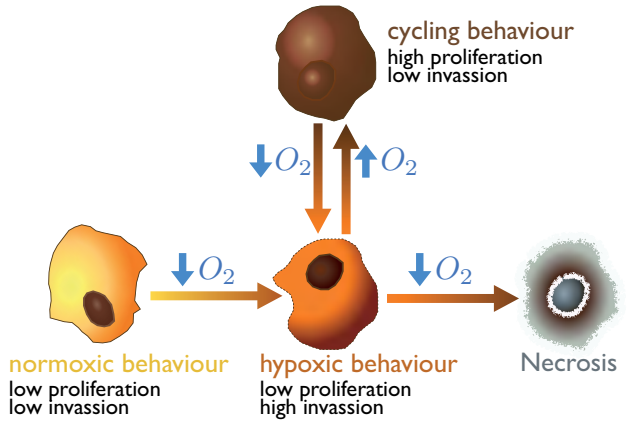

Figure 2: Graphical depiction of the mathematical model scheme based on previous models [5, 7] including 3 cancer cell phenotypes, the oxygenation and the necrosis.

The pseudapalisades formation hypothesis was previously studied from our group considering only vessel obstruction events [4]. Nutrient and oxygen starvation triggered a strong migratory process leading to pseudopalisade generation in silico and in vitro [4, 7, 8]. Also, cells at greatest distance from oxygen supply became hypoxic after a critical point in tumor growth was reached (due to increased metabolism) forming pseudopalisades both in silico and in vitro.

The aim of this research is to study the pseudopalisades formation hypothesis considering chronic hypoxia conditions under high tumor cell densities and to combine and analyze the results coming from both hypothesis.

2 Materials and Methods

2.1 Mathematical model

This model is based on our previous models in which oxygen coming from straight vessels was the driving force that triggered the normoxic and hypoxic phenotypic changes [7, 8]. To these 2 dominant phenotypes, based on the go-or-grow dichotomy, we have incorporated a third phenotype accounting for hypoxic cells that arrive to normoxic areas and switch to a more proliferative phenotype. Thus, the model is a hybrid between go-or-grow and go-and-grow models.

In addition to the diffusive random motion, we have included a directional transport term driving the cell′s motion towards better oxygenated regions for hypoxic cells. The Fig. 2 exhibits a graphical representation for the model of pseudopalisades formation.

The mathematical model consists of a set of partial differential equations modeling the interplay of 3 cellular cancer cell phenotypes, the oxygen distribution and necrosis.

Major Assumptions of the Mathematical Model:

1. Classical logistic space limited growth for the tumor cell densities: Normoxic C_n, Hypoxic C_h, Malignant C_m and Necrotic C_d.

2. Coefficient diffusion for hypoxic phenotype, D_h is higher than the normoxic D_n and the malignant D_m (D_h>D_n>D_m).

3. Cell duplicating time for hypoxic phenotype, τ_h is higher than the normoxic τ_n and the malignant τ_m. Malignant cells have the highest proliferation (τ_h>τ_n>τ_m).

4. Oxygen O_2 acts as a chemoattractant for hypoxic cells with a hypoxic transport coefficient T_h.

5. Oxygen diffusion D_{O_2} is homogenous and isotropic in the chamber. Oxygen flows from channels to balance the different oxygen pressures.

6. Malignant cells consume more oxygen than any other cell phenotype: $\alpha_m > \alpha_n > \alpha_h$ where α_n and α_h are the rate of oxygen consumption for normoxic and hypoxic cells respectively.

7. Depending on the oxygen pressures various switching mechanisms arise coupling the populations: Normoxic to hypoxic S_{nh} below $O_2^{(S)}$ pressure with characteristic time τ_{nh}. Hypoxic to malignant S_{hm} above $O_2^{(S)}$ with characteristic time τ_{hm}. Malignant to hypoxic S_{mh} below $O_2^{(S)}$ with characteristic time τ_{mh}. Hypoxic to necrotic S_{hd} below $O_2^{(D)}$ with characteristic time τ_{hd}. (We consider S_{nh}=S_{mh}).

The equations governing the interplay between the dominant phenotypes are displayed in Eqs. 1.

$$(1)\quad \begin{cases} \frac{\partial C_n}{\partial t} = D_n \nabla^2 C_n + \frac{C_n}{\tau_n} D - \frac{S_{nh}}{\tau_{nh}} C_n, \\ \frac{\partial C_h}{\partial t} = D_h \nabla^2 C_h + \frac{C_h}{\tau_h} D + T_h \nabla O_2 \left(\frac{\partial C_h}{\partial x}\right) \\ \qquad + \frac{S_{nh}}{\tau_{nh}} C_n - \frac{S_{hm}}{\tau_{hm}} C_h + \frac{S_{mh}}{\tau_{mh}} C_m - \frac{S_{hd}}{\tau_{hd}} C_h, \\ \frac{\partial C_m}{\partial t} = D_m \nabla^2 C_m + \frac{C_m}{\tau_m} D - \frac{S_{mh}}{\tau_{mh}} C_m + \frac{S_{hm}}{\tau_{hm}} C_h \\ \frac{\partial C_d}{\partial t} = \frac{S_{hd}}{\tau_{hd}} C_h. \end{cases}$$

Where $D = 1 - \frac{C_n + C_h + C_m + C_d}{C^M}$ and C^M is the maximum number of tumor cells where ΔO_2 is the oxygen sensitivity threshold.

The explicit form of the switch functions are represented in Eq.[2- 4].

$$(2)\quad S_{mh} = S_{nh} = \frac{1}{2}\left[1 - \tanh\left(\frac{O_2 - O_2^{(S)}}{\Delta O_2}\right)\right],$$

$$(3)\quad S_{hm} = \frac{1}{2}\left[1 + \tanh\left(\frac{O_2 - O_2^{(S)}}{\Delta O_2}\right)\right],$$

$$(4)\quad S_{hd} = \frac{1}{2}\left[1 - \tanh\left(\frac{O_2 - O_2^{(D)}}{\Delta O_2}\right)\right].$$

Eq.5 represents the spatio-temporal evolution of oxygen.

$$(5)\quad \frac{\partial O_2}{\partial t} = D_{O_2} \nabla^2 O_2 - \frac{\alpha_n C_n + \alpha_h C_h + \alpha_m C_m}{O_2^{(T)} + O_2} O_2 + J$$

The first term in the right-hand-side of Eq.5, accounts for oxygen diffusion, the second term models the oxygen consumption by both normoxic and hypoxic cells. The saturation Michaelis-Menten constant $O_2^{(T)}$ corresponds to the oxygen pressure level at which the reaction rate is halved. The third term describes the oxygen flow from the vessels (channels) to the tissue (chamber).

The multiplicative function J in Eq. 5 accounts for the spatial distribution of the oxygen supply and depends on the blood vessels positions (channels) p_i, their oxygenation $O_2^{v_i}$ and their sizes v_i. In Eq.6, i refers to the number of channels and J will be taken to be a combination of Gaussian functions of the form

$$(6)\quad J = (O_2^{v_i} - O_2) J_{O_2} \sum_{i=1}^{N} e^{-(x-p_i)^2/v_i^2}$$

Where p_i and v_i represent the position and size of the vessel. J_{O_2} is the flux of oxygen coming from the vessel ($10^{-6}\ s^{-1}$ estimated).

2.2 Microdevice design, fabrication and operation

Microfluidic devices were fabricated using SU-8 photolithography combined with an SU-8 to SU-8 bonding process. The fabrication process was inspired by previously reported work [6, 5].

In order to recreate obstructed conditions in a 1000 μm wide central microchamber, a regular flow of culture media was provided to the microdevice through one lateral, whereas the other was sealed [4].

In order to recreate the chronic hypoxia under high cellularity conditions, the microdevices have been designed including a 2000 μm wide central microchamber to allocate the hydrogel with the cells embedded and two flanking 700 μm wide lateral microchannels. The internal microdevice height was 250 μm and dedicated inlets and outlets have been also integrated to enable user-friendly liquid insertion by manual pipetting. Hydrogel with the cells embedded was confinement in the central microchamber thanks to a series of parallelogram-shaped pillars. Fabrication was performed by injection molding using polystyrene as structural material. After isopropanol washing, they were bonded to the surface of a 60 mm diameter Petri dish using biocompatible adhesive (adhesive research, ARcare 8026) to create a functional microdevice. Microdevices were finally sterilized by submerging in 70% ethanol. Microfluidic devices for cell culture were finally ready after dried inside the culture hood O/N.

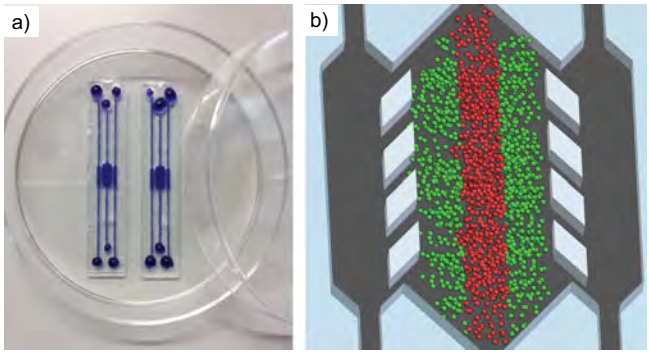

Figure 3: a) Two microfluidic devices for cell culture where blue-colored water was perfused for visualization purposes. b) Experimental scheme within the microdevice mimicking the hypoxic conditions and the starved (red) and well oxygenated (green) regions. The experiments developed reproduce: (i) obstructed blood vessel conditions and (ii) high cellularity under unrestricted conditions.

2.3 Cell culture

U-251-MG cells were acquired from ATCC and routinely grown in Dulbecco's modified Eagle's medium (DMEM)

(Lonza BE12-614F) supplemented with 10% v/v fetal bovine serum (Sigma F7524) and antibiotics (penicillin/streptomycin, Lonza DE 17-602E) at 37°C and 5% CO2 in a TEB-1000 incubator (EBERS Medical Technology). To embed the cells in a 3D collagen hydrogel, all reagents, were located on ice to prevent the collagen polymerization. Cells were detached using a trypsin/EDTA solution (Lonza, CC-5012) and resuspended in a calculated volume of growth medium (DMEM supplemented with 10 % fetal bovine serum) in order to reach the final desired concentration.

For experiments mimicking the obstructed conditions: using a chilled tip, we prepared a mixture of 24.9 μl of collagen type I 4.01 mg/ ml (Corning 354236), 0.62 μl of NaOH 1N (Sigma 655104), 10 μl of DMEM 5X (Sigma D5523), 50 μl of cell solution, and 14.5 μl of sterile water. For experiments mimicking the high cellularity conditions: We prepared a mixture of 3.4 μl of sterile water; 35.7 μl of collagen type I 3.36 mg/ml (Corning 354236); 0.89 μl of NaOH 1N (Sigma 655104); 10 μl of DMEM 5X (Sigma D5523) and 50 μl of cell solution.

Finally, the hydrogel mixture was injected into the microdevice by manual pipetting. To allow the collagen polymerization, the microdevices were placed into an incubator (37°C and 5% CO2) for 15 minutes.

2.4 Cell Viability

Cell viability was analyzed using Calcein (CAM) (Life technologies C1430) and propidium iodide (PI) (Sigma P4170). Stocks solutions were prepared following supplier instructions. CAM and PI working solutions were prepared diluting both stock solutions in PBS (Lonza BE17-516F) at a final concentration of 5μ g/ml CAM and 4 μ g/ml PI respectively. Before injecting the CAM/PI cocktail, microdevices were washed once with PBS. CAM labelled viable cells in green, whereas PI labelled only dead cells in red. Confocal images were taken after 30 min using a Nikon Eclipse Ti microscope equipped with a C1 modular confocal microscope system. 2X magnification images were taken and Z-stacks were collected at different focal planes using 10 microns steps with the 10X.

2.5 Image analysis

Image analysis was performed using Fiji software ((http://fiji.sc/Fiji). Viable cell distribution was analyzed across the central microchamber in the 10X magnification. Viable cell distribution was quantified only on the 10X images since in the 2X the Z resolution was not enough to distinguish cell located at different planes, visualizing all the microchamber height as a projection of all of them. This caused that changes in cell density did not correlate linearly with the cell occupied area. Although in 10X this phenomenon is still present, its effect is much lower.

3 Parameter estimation

To solve the mathematical model numerically we have used a standard finite difference method of second order in time and space.

The value of the parameters used in the model were equal or very similar to those used in [4, 8] except for the parameters displayed in Table 1.

Table 1

Parameter	Value and units	Meaning
τ_{mh}	12 h	Malignant to hypoxic phenotype switch time
τ_{hm}	7 days	Hypoxic to malignant phenotype switch time
α_m	$25\alpha_n$ mmHg c/s	Typical malignant cell oxygen consumption
D_m	2×10^{-10} cm^2/s	Malignant diffusion coefficient
T_h	7×10^{-9} cm^2/s	Hypoxic transport coefficient
τ_m	48h	Malignant doubling time

4 Results and discussion

4.1 Pseudopalisade formation under obstructed conditions

The pseudopalisade formation under obstructed conditions is based on the idea that GBM proliferation and secretion of procoagulant signals would causes thrombotic events leading to acute hypoxia. Then, the migration of cells away from a thrombosis and towards nutrients and oxygen enriched regions could create the pseudopalisades. In addition, these migrating cells would reach other blood vessels and eventually cause their collapse, restarting the process and creating another expanding wave of tumor cells within the brain.

Our mathematical simulations support the hypothesis of pseudopalisade formation after a vessel-occlusion event and correlate very well with microfluidic device experiments in which we saw an increase in the cell proliferation when the cells where exposed to obstructed conditions (Fig. 4).

Our results suggest that when these invading and hypoxic GBM cells reach a better oxygenated region, they start to proliferate more aggressively.Therefore, microscopic hypoxic events can act as a driving force in GBM invasion [4]. Therefore, this mathematical model is able to recapitulate the pseudopalisade formation as a hypoxia-driven phenomenon, convincingly reproducing the observed results within the microdevice and the observed pseudopalisades in vivo [4].

Fig. 4 presents the experimental data versus the computer simulations of the evolution of the 4 millions U-87 cells seeded within the 1 mm chamber. Red, blue and black curves refer to day 3, 6, 9.

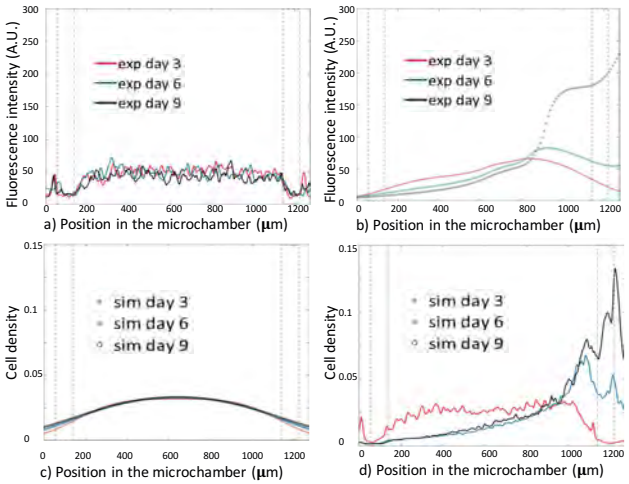

Figure 4: Experimental data versus computer simulations of the cell evolution within the chamber at days 3, 6, and 9. a) Experimental data of green fluorescence intensity under unrestricted conditions. b) Experimental data of green fluorescence intensity under restricted conditions. c) Simulations of alive tumor cell density evolution under unrestricted conditions. d) Simulations of alive tumor cell density evolution under restricted conditions.

4.2 Pseudopalisade formation under high cellularity conditions

diferecias y transicion

The pseudopalisade formation under high cellularity conditions is based on the idea that the high GBM density itself within the brain tissue causes oxygen and nutrient deprivation to those cells away from the vessels even when they still working properly. Those, pseudopalisades could develop without any external input.

Cell viability within the central microchamber was analyzed at different cell densities and different times. The analysis revealed that at 4 and 10 million cells/ml no significant changes were observed in cell viability or cell distribution. Interestingly, at 20 million cells/ml a moderate change in the cell distribution is observed, whereas at 40 million cells/ml this effect is much more evident.

The Fig. 5 exhibits the experimental results for 4 millions and 40 millions cells. The green fluorescence represents alive cells while the red label death cells. Fluorescence intensity was measured in adimensional units. Green fluorescence for day 0, 1, 2, 3, 6 is presented in blue, red, green, purple and orange curves respectively along the right side of the chamber.

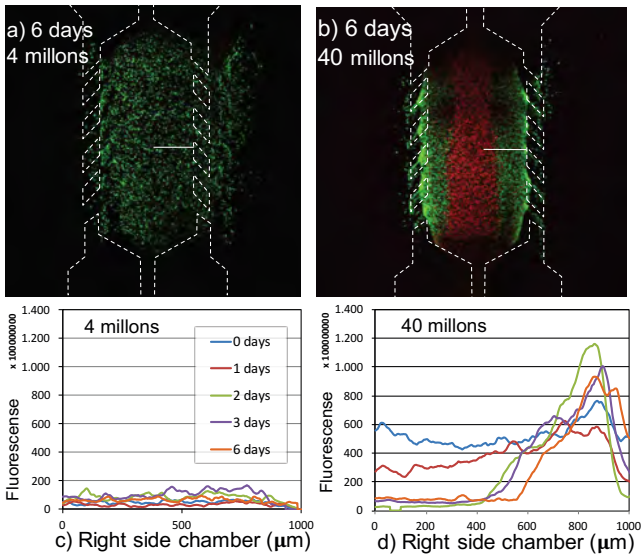

Figure 5: Chronic hypoxia experiment developed within the microfluidic device. After 6 days live cells are labeled in green and death cells in red. a) 4 million U-251/ml in 1,2 mg/ml collagen hydrogel. Microdevice posts are delimited in white dashed line. b) 40 million U-251/ml in 1,2 mg/ml collagen hydrogel. c) Green fluorescence intensity along the right side chamber at day 0, 1, 2 ,3 and 6 considering 4 millions tumor cells at day 0. d) Green fluorescence intensity along the right side chamber at day 0, 1, 2 ,3 and 6 considering 40 millions tumor cells at day 0.

We developed computational simulations considering a physiological range for the unknown parameters and the typical results obtained are presented in Fig. 6. We related the 0.04 initial cell density with the 4 millions experiment and 0.4 initial cell density with the 40 millions experiment.

Pseudopalisades were not observed under initial cell densities below 0.1-0.2 (Fig. 6 a)-d)). Simulations with initial cell densities between 0.2-0.6 showed a wave of cells moving from the center of the chamber to the channel (Fig. 6 e)-h)). Both facts are consistent with the experimental data and the pseudopalisades formation caused by chronic conditions.

In addition, the mathematical results for initial cell densities above 0.6 showed a pseudopalisade formed by static cells where basically cells in the center of the chamber die because of the starvation (Fig. 6 i) and j)).

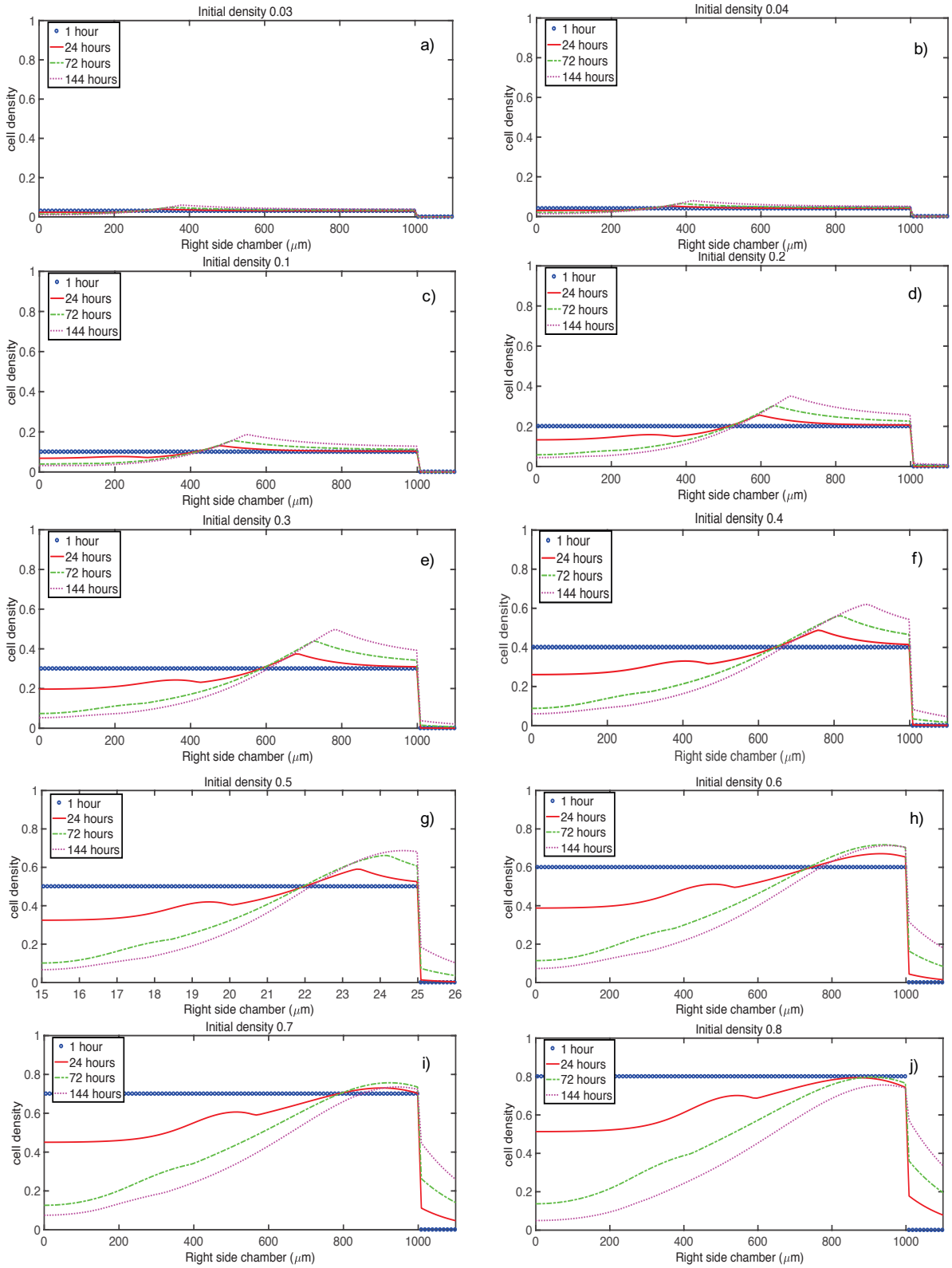

Figure 6: Computational simulation evolution of the cell density within the right side of the chamber after 1 hour, 1 day, 3 days and 6 days (in blue, red, green and purple curves respectively). Initial alive cell densities are: a) 0.03, b) 0.04, c) 0.1, d) 0.2, e) 0.3, f) 0.4, g) 0.5, h) 0.6, i) 0.7 and j) 0.8.

Our mathematical simulations and experiments support the hypothesis of pseudopalisade formation under an elevated number of cells in a tissue with functional vessels.

Also suggest that this pseudopalisades are formed by waves of migrating cells only when cell density is below ≈0.6. If cell density is above 0.6, it would be possible to find pseudopalisades but they would not be formed by migrating cells and they could not imply invasiveness.

The mathematical model suggests that pseudopalisades formed by ways of cells and caused by an increment in cellularity will only take place if the tissue cell density under healthy conditions is low enough (below 0.6). This could be one of the reasons why pseudopalisades as a signal of invasion are almost exclusive from GBM cells. Following the results, in tissues with cellularity over 0.6, pseudopalisades would not be formed by migrating cells and their formation could not be associated with an accelerated invasion.

5 Conclussion

The pseudopalisade formation under obstructed conditions hypothesis proposes that GBM cells are exposed to cyclic starvation which forces their metabolism to switch between a proliferative or migrating phenotype. The pseudopalisade formation under high cellularity conditions hypothesis proposes that GBM cells away from nutrients and oxygen supply move towards better oxygenated regions.

A mathematical model was developed incorporating the main mechanisms of pseudopalisade formation. All the elements included in the mathematical model were necessary to describe both types of phenomena (acute and chronic hypoxia) pointing out to the insufficiency of the go-or-grow hypothesis to describe pseudopalisade formation on-chip.

Using a combination of computational and experimental techniques, we proved the feasibility of the two hypotheses of pseudopalisade formation, driven by either acute or chronic hypoxia. Our mathematical model suggest that pseudopalisades caused by high cellularity are formed by waves of moving cells only if cell density is below ≈0.8. If cell density is above 0.6, it would be possible to find pseudopalisades but they would not be formed by migrating cells and they could not imply invasiveness.

Additionally, we verified the potential of microfluidic devices as advanced artificial systems capable of experimentally modeling nutrient and oxygen gradients during tumor evolution.

Acknowledgements

National Research Program, Spain (BIO2016-79092-R, DPI2015-65401-C3-1-R, MTM2012-31073, bes-2012-059940, PI12/00775, PI13/01258 and RD12/0036/0027); FEDER Spain [MTM2015-71200-R]. Junta de Comunidades de Castilla-La Mancha, Spain [PEII-2014-031-P]. James S. Mc. Donnell Foundation, USA (220020420 and 220020450). Morgridge Institute for Research, Postdoctoral fellow program.

References

[1] T. Oike, Y. Suzuki, K. Sugawara, et al. *Radiotherapy plus concomitant adjuvant temozolomide for glioblastoma: Japanese mono-institutional results.* PloS one. 2013; 8(11):e78943.
https://doi.org/10.1371/journal.pone.0078943

[2] Y. Rong, D.L. Durden, E.G. Van Meir, D.J. Brat. *'Pseudopalisading' necrosis in glioblastoma: a familiar morphologic feature that links vascular pathology, hypoxia, and angiogenesis.* Journal of neuropathology and experimental neurology. 2006; 65(6):529-539.
https://doi.org/10.1097/00005072-200606000-00001

[3] D.J. Brat, A.A. Castellano-Sanchez, S.B. Hunter, et al. *Pseudopalisades in glioblastoma are hypoxic, express extracellular matrix proteases, and are formed by an actively migrating cell population.* Cancer research. 2004; 64(3):920-927.
https://doi.org/10.1158/0008-5472.CAN-03-2073

[4] J.M. Ayuso, R. Monge, A. Martínez-González, M. Virumbrales-Muñoz, G.A. Llamazares, J. Berganzo, A. Hernández-Laín, J. Santolaria, M. Doblaré, C. Hubert, J.N. Rich, P. Sánchez-Gómez, V.M. Pérez-García, I. Ochoa and L.J. Fernández. *Glioblastoma on a microfluidic chip: Generating pseudopalisades and enhancing aggressiveness through blood vessel obstruction events.* Neuro Oncol. 2017. doi: 10.1093/neuonc/now230.
https://doi.org/10.1093/neuonc/now230

[5] J.M. Ayuso, R. Monge, G. Llamazares, et al. *SU-8 based microdevices to study self-induced chemotaxis in 3D microenvironments.* Front Mater. 2015;2:37.
https://doi.org/10.3389/fmats.2015.00037

[6] F.J. Blanco, M. Agirregabiria, J. Garcia, et al. *Novel three-dimensional embedded SU-8 microchannels fabricated using a low temperature full wafer adhesive bonding.* J Micromech Microeng. 2004;14(7):10.
https://doi.org/10.1088/0960-1317/14/7/027

[7] A. Martínez-González, G.F. Calvo, L.A. Pérez Romasanta, V.M. Pérez-García. *Hypoxic cell waves around necrotic cores in glioblastoma: a biomathematical model and its therapeutic implications.* Bull Math Biol. 2012;74(12):2875-2896.
https://www.ncbi.nlm.nih.gov/pmc/articles/PMC3510407/

[8] A. Martínez-González, M. Durán-Prado, G.F. Calvo, F.J. Alcaín, L.A. Pérez- Romasanta, V.M. Pérez-García. *Combined therapies of antithrombotic sand antioxidants delay in silico brain tumour progression.* Math Med Biol. 2015;32(3):239-262
https://www.ncbi.nlm.nih.gov/pubmed/24562299